

# Bose-Einstein-Condensation

## Observation and Application

Gerd Friemel

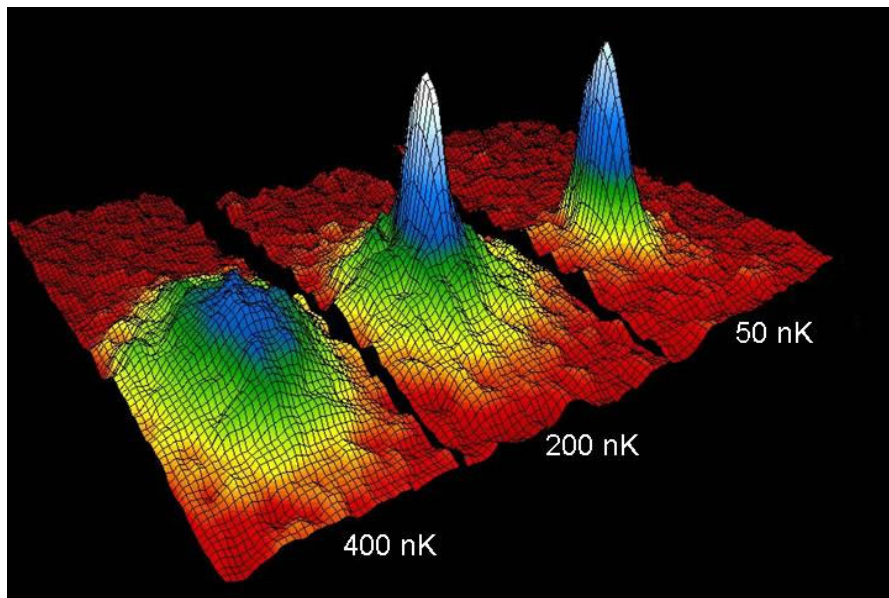
Tutor: Dr Binoy Sobnack

Loughborough University

Department of Physics

Winter term 08/09

30/01/2009



# Bose-Einstein-Codensation

## Contents

<b>1</b>	<b>The Prediction of Bose-Einstein Condensation</b>	<b>3</b>
1.1	Ideal Fermion-and Boson-Gas . . . . .	3
1.2	Thermodynamics of fermions and bosons . . . . .	5
1.3	Quantitative description of BEC . . . . .	6
<b>2</b>	<b>Experimental Realization of BEC</b>	<b>9</b>
2.1	Laser-Cooling . . . . .	10
2.2	Magnetic trapping . . . . .	14
2.2.1	Applied magnetic field and evaporative cooling . . . . .	16
2.3	Observation of BEC . . . . .	18
<b>3</b>	<b>Subsequent experiments</b>	<b>19</b>
3.1	Observation of BEC in a gas of sodium atoms . . . . .	19
3.2	Observation of interference between two Bose condensates . . . . .	20
3.3	Superradiant Rayleigh Scattering from a Bose-Einstein Condensate . . . . .	21

<sup>1</sup>from <http://jila-www.colorado.edu/bec/> (JILA)

## Introduction

With the development of quantum physics at the beginning of the 20th century a different view on thermodynamics was prompted. While an ideal gas with infinitesimally small and interaction-free particles was well understood, new properties like quantum state or wavefunction and quantity of total spin had to be taken into account, the latter classifying particles in either bosons or fermions. Boson with integer spin can multiply occupy one state in a given quantum system, whereas it is forbidden for fermion with half-integer to occupy the same state twice. For a Bose-gas obeying the Bose-Einstein statistics it is therefore possible to condensate completely into one quantum state, where particles behave identically. This is called a Bose-Einstein condensate, which was postulated already in 1925. The experimental prove was, however, more difficult. At high temperatures a boson gas behaves nearly like an ideal gas, because the mean distance between particles is sufficiently large. Because of the Bose-Einstein-statistics, it is nearly impossible that a macroscopically number of particles are in the same quantum state at the same time. The only way to achieve this would be to gradually remove energy of the system until all particles are forced into the lowest energy state. This requires low temperature, which with the experimental techniques at that time could not be attained. There were of course hints that Bose-Einstein condensation exists with the discovery of superconductivity in 1911 and superfluidity in 1937 and their subsequent microscopically explanations, which stated that particles condense in one quantum state. But these theories involved interaction between atoms, which was contrary to the prediction of Bose and Einstein, where non-interactive atoms condense. The first true Bose-Einstein-condensation was yet to be shown. Finally, in 1995 a group from of the University of Colorado at Boulder NIST-JILA successfully observed BEC in  $^{87}\text{Rb}$ , utilizing new technologies in laser cooling and magnetic trapping. But the effort is not diminished through this fulfilment, since many properties have to be examined and condensates of different elements have to be produced. And of course BEC provides the key for the development of the atom laser and its application, which is still in the beginning.

## 1 The Prediction of Bose-Einstein Condensation

### 1.1 Ideal Fermion-and Boson-Gas

At high temperatures, e.g. room temperature, gases like  $^4\text{He}$  or  $^3\text{He}$  follow the Maxwell-Boltzmann-Distribution. The average occupation of an energy state  $\varepsilon_i$  is expressed by the formula:

$$\bar{n}_i = g_i e^{-\frac{\varepsilon_i - \mu}{kT}} \quad (1)$$

with:

- $g_i$  degeneracy of state
- $\mu$  chemical potential
- $k$  Boltzmann constant
- $T$  temperature
- $N$  total number of particles

This formula only applies for the case of dilute gases and high temperatures. This means that the mean distance between particles is much greater than the de Broglie wavelength,  $\sqrt[3]{V/N} \gg \lambda$ . At lower temperatures this condition cannot be held any more because the De Broglie-wavelength increases with decreasing temperature as  $\lambda \sim \frac{1}{\sqrt{T}}$ . In other words, because of the fact that at lower temperatures high energy states are frozen out, it gets more and more improbable for particles to occupy high energy states according to (1). At this point we have to take quantum effects like the Pauli exclusion principle into account which considers the fact that identical particles are indistinguishable. It postulates that particles with half-integer spin, called fermions, cannot occupy the same quantum state simultaneously, whereas integer spin particles, called bosons, can. This proposition leads to the application of antisymmetric or symmetric many particle wavefunctions when dealing with quantum gases which contain either fermions or bosons. In general, such wavefunctions can be described in the following way when neglecting interaction between particles.

Antisymmetric and symmetric wavefunctions must behave antisymmetrically and symmetrically under transposition of coordinates, respectively:

$$P_{ij}\psi_A = -\psi_A, \quad \text{for fermions} \quad (2)$$

$$P_{ij}\psi_S = \psi_S, \quad \text{for bosons} \quad (3)$$

A system with N particles can be described by its configuration, where  $\nu_1, \nu_2, \dots$  are one-particle-states, derived from the Schroedinger equation for one particle.

$$c = \{\nu_1, \nu_2, \nu_3, \dots, \nu_n\} \quad (4)$$

The normal multiplied wavefunction  $\Psi_c = \Phi_{\nu_1}(x_1)\Phi_{\nu_2}(x_2)\dots\Phi_{\nu_N}(x_N)$  would not satisfy (3), so it has to be modified. Especially for the antisymmetric case the Slater-Determinate is used to fulfil the demand of the Pauli-Principle. Thus, if two states in the configuration are equal, then two rows in the Slater-determinant are identical and the value collapses to zero which implies a forbidden state of the system.

Here the many particle wavefunction:

$$\Psi_c^A = \frac{1}{\sqrt{N!}} \begin{vmatrix} \Phi_{\nu_1}(x_1) & \Phi_{\nu_1}(x_2) & \dots & \Phi_{\nu_1}(x_N) \\ \Phi_{\nu_2}(x_1) & \Phi_{\nu_2}(x_2) & \dots & \Phi_{\nu_2}(x_N) \\ \dots & \dots & \dots & \dots \\ \Phi_{\nu_N}(x_1) & \Phi_{\nu_N}(x_2) & \dots & \Phi_{\nu_N}(x_N) \end{vmatrix} \quad (5)$$

$$\Psi_c^S = \frac{1}{\sqrt{N!}} \frac{1}{\sqrt{n_1! n_2! \dots n_N!}} \sum_{P \in S_N} T_P \{ (\Phi_{\nu_1}(x_1) \Phi_{\nu_2}(x_2) \dots \Phi_{\nu_N}(x_N)) \} \quad (6)$$

In the symmetric wavefunction the sum goes over all possible permutations of coordinates. Multiple occupation is possible.

## 1.2 Thermodynamics of fermions and bosons

The microstate  $\alpha$  of a system of bosons and fermions is described in the same way as above.

$$\alpha = \{n_0^\alpha, n_1^\alpha, \dots\}$$

Where  $n_i^\alpha$  is the occupation number of a one-particle state  $i$ . Since the partition function  $Z$  is the starting point for any thermodynamic considerations, it should be calculated at first. This is possible only through assuming that the system is a grand canonical ensemble.

$$Z(T, V, \mu) = \sum_{\alpha} e^{\beta(\mu N_{\alpha} - E_{\alpha})} \quad \text{and :} \quad (7)$$

$$N_{\alpha} = \sum_i n_i \quad (8)$$

$$E_{\alpha} = \sum_i \varepsilon_i n_i \quad (9)$$

Therefore:

$$Z = \sum_{\alpha} e^{\beta \sum_i n_i (\mu - \varepsilon_i)} = \prod_i \sum_{n_i} e^{\beta(\mu - \varepsilon_i) n_i} \quad (10)$$

In the last term the summation over the occupation number  $n_i$  can be performed until infinity because the total particle number is not restricted. Considering only one factor of the above product, one can get:

$$\begin{aligned} Z_i^F &= 1 + e^{\beta(\mu - \varepsilon_i)}, & \text{because for fermions : } n_k &= 0, 1 \\ Z_i^B &= \frac{1}{1 - e^{\beta(\mu - \varepsilon_i)}}, & \text{because for bosons : } n_k &= 0, \dots, \infty \end{aligned}$$

The total partition sum  $Z$  is related to the grand potential  $\Omega$  in the following way:

$$\begin{aligned} \Omega^F(T, V, \mu) &= -kT \ln Z^F = -kT \sum_i \ln(1 + e^{\beta(\mu - \varepsilon_i)}) \\ \Omega^B(T, V, \mu) &= -kT \ln Z^B = kT \sum_i \ln(1 - e^{\beta(\mu - \varepsilon_i)}) \end{aligned} \quad (11)$$

With the useful formula (12) one can derive the expressions for Fermi-Dirac and Bose-Einstein-distribution which are very important in discussing quantum gases.

$$\bar{n}_i = \frac{1}{\beta} \frac{\partial}{\partial \epsilon_i} \ln Z \quad (12)$$

$$\langle n_i^F \rangle = \frac{1}{e^{\beta(\epsilon_i - \mu)} + 1}, \quad \text{Fermi - Dirac} \quad (13)$$

$$\langle n_i^B \rangle = \frac{1}{e^{\beta(\epsilon_i - \mu)} - 1}, \quad \text{Maxwell - Boltzmann}$$

The average occupation number for fermion fulfils  $0 < \langle n_i^F \rangle < 1$  which is evident from the equations above. The case for bosons is more interesting. Averting the unphysical solution with occupation numbers  $\langle n_i^B \rangle < 0$  for all energy levels, especially the lowest level  $\epsilon_0$ , leads to the constraint  $\mu < \epsilon_0$ . But this does not forbid an evolution, where  $\mu \rightarrow \epsilon_0$ . In this case the occupation number of the lowest energy state attains macroscopic dimensions; Bose-Einstein condensation is obtained.

### 1.3 Quantitative description of BEC

To compute the total number of Bose-particles, we make use of the plausible relation:

$$N(T, V, \mu) = \sum_i \bar{n}_i \quad (14)$$

For simplicity the particles can be described as plane waves in a box of volume  $V$ .

$$\phi_{\mathbf{p}} = \frac{1}{\sqrt{V}} e^{i\mathbf{p}\cdot\mathbf{r}/\hbar} \quad (15)$$

$$\text{with : } \mathbf{p} = 2\pi\hbar\mathbf{n}/L, \quad \mathbf{n} = (n_x, n_y, n_z)$$

Consequently, the states are densely packed in p-space. One state takes up the volume  $\Delta p = \hbar^3 \frac{(2\pi)^3}{V}$ . If the volume is large enough, the distribution of states in p-space can be treated as being continuous. In that way a summation over all possible energy levels can be converted into an integration  $\sum_{\mathbf{p}} \rightarrow V/(2\pi\hbar)^3 \int d^3\mathbf{p}$ . Since in (13) only the energy value appears, it is practicable to perform the integration over the energy. The ground level in this consideration is found at zero point ( $\epsilon_0 = 0$ ). Making use of the dispersion relation  $\epsilon = \frac{p^2}{2m}$  which applies to all massive particles, we can finally

compute the particle number with the help of (13, 14).

$$\begin{aligned}
 d\varepsilon &= \frac{d\varepsilon}{dp} \cdot dp = \sqrt{\frac{2\varepsilon}{m}} dp \\
 V/(2\pi\hbar)^3 \int d^3p &\longrightarrow 4\pi \frac{V}{h^3} \int p^2 \cdot dp \longrightarrow \frac{4\pi V}{h^3} \sqrt{2} m^{3/2} \int_0^\infty \sqrt{\varepsilon} d\varepsilon \\
 \text{therefore : } N &= \frac{V}{\lambda_T^3} \cdot \frac{2}{\sqrt{\pi}} \int_0^\infty dx \sqrt{x} \frac{1}{z^{-1}e^x - 1} \\
 \text{with : } \lambda_T &= \sqrt{\frac{2\pi\hbar^2}{mk_B T}}, \quad \text{thermal wavelength} \\
 z &= e^{\beta\mu}, \quad \text{is called fugacity} \\
 \Gamma(p) &= \int_0^\infty x^{p-1} e^{-x} dx, \quad \text{factorial function} \quad (16)
 \end{aligned}$$

The integral in (16) corresponds to function  $g_{3/2}(z)$  which belongs to a special class of functions, called Bose functions.

$$\begin{aligned}
 g_p(z) &= \frac{1}{\Gamma(p)} \int_0^\infty dx x^{p-1} \frac{1}{z^{-1}e^x - 1} = \sum_{l=1}^\infty \frac{z^l}{l^p} \\
 \text{thus : } N_T &= \frac{V}{\lambda_T^3} g_{3/2}(e^{\beta\mu}) \quad (17)
 \end{aligned}$$

This function depends only on the chemical potential  $\mu$  through the fugacity  $z$ . In the above derivation for the particle number  $N$  the behaviour of the ground level  $\varepsilon$  was neglected. In the transition to a continuous sum, the contribution of this level to the total sum is infinitesimally small. This is correct for small occupation numbers at high temperatures, but incorrect in the case of macroscopic condensation into this state. Therefore, we have to write the particle number as a sum of ground state  $N_0$  and excited state occupation  $N_T$ . The latter was derived above.

$$N = N_0 + N_T \quad (18)$$

The occupation of the  $\varepsilon_0$  depends on  $\mu$  as well. Assume that the state has  $N_{cond}$  particles. Making use of formula (13) and substituting  $\langle n_0^B \rangle = N_{cond}$  one can estimate:

$$\mu \approx \frac{-kT}{N_{cond}} \quad (19)$$

Hereby, it is shown that the chemical potential follows the  $\mu \rightarrow \varepsilon_0 = 0$  development. The exact value of  $\mu$  is defined by equation (18). With the knowledge of (18,16) we can finally plot the function  $N_0(\mu), N_T(\mu)$ .

While  $N_0$  diverges at  $\mu = \varepsilon_0$ ,  $N_T$  reaches its maximum  $N_c$  at this point, with  $N_c \sim T^{3/2} g_{3/2}(1)$ , ( $\varepsilon_0 = 0$ ). Thus, the non-consideration of the ground state and

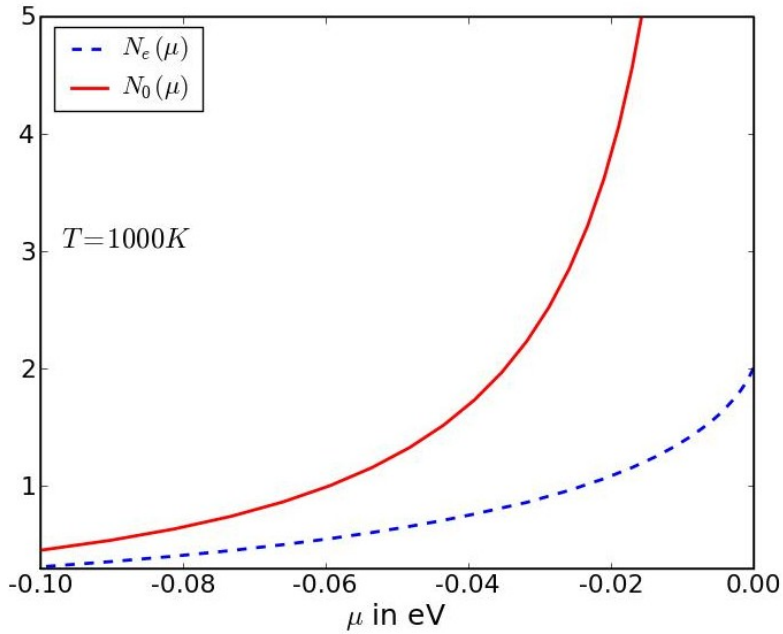


Figure 1: Variation of  $\mu$  at fixed temperature

its occupation is only possible as long as  $N_c > N$ . Below a critical temperature  $T_c$  the condition, that almost all particles are excited, can not be held anymore, and Bose-Einstein-condensation inevitably takes place. With formula (17) we obtain  $T_c$  by setting  $\mu = 0$  and evaluating the integral.

$$T_c = \frac{h^2}{2\pi m k} \left( \frac{n}{2.612} \right)^{2/3}, \quad n = \frac{N}{V} \quad (20)$$

Since in the case of  $T < T_c$ ,  $\mu = 0$  is valid throughout the range, the number of excited particles can be written in simplified form, still in accordance to (17).  $N_0$  follows instantly from the normalization condition.

$$N_T = \left( \frac{T}{T_c} \right)^{3/2} \cdot N \quad (21)$$

$$N_0 = N \left[ 1 - \left( \frac{T}{T_c} \right)^{3/2} \right]$$

These formulae were deduced under the assumption, that above  $T_c$  the number of particles in the ground state can be neglected. In the same way like done with  $N$ , an

expression for inner energy  $E$  can be obtained.

$$\begin{aligned}
 E &= \sum_i \frac{\varepsilon_i}{e^{\beta(\varepsilon_i - \mu)} - 1} & (22) \\
 \rightarrow E &= \frac{3}{2} \cdot k_B T \frac{V}{\lambda_T^3} \frac{4}{3\sqrt{\pi}} \int_0^\infty x^{3/2} \frac{1}{z^{-1}e^x - 1} \\
 &= \frac{3}{2} \cdot k_B T \frac{V}{\lambda_T^3} g_{5/2}(z), \quad \text{for } T > T_c \\
 E &= \frac{3}{2} k_B T \frac{V}{\lambda_T^3} g_{5/2}(1), \quad \text{for } T \leq T_c, \quad g_{5/2}(1) = 1.342
 \end{aligned}$$

According to equation (20) the critical temperature only depends on the particle density and the mass. Taking for example gaseous  ${}^4\text{He}$  at its boiling point, the result is  $T_c = 0.5\text{ K}$ . Far in the range of liquid  ${}^4\text{He}$ . The same calculation, this time with the mass density of  $0.14\text{ g/cm}^3$ , yields  $T_c = 3.1\text{ K}$ , which is in the vicinity of the  $2.17\text{ K}$ , the  $\lambda$ -point. This coincidence has led to assumption, that the phenomenon of superfluidity of liquid  ${}^4\text{He}$  is in fact a Bose-Einstein-condensation.

For describing a mixed system of condensed and excited particles quantum mechanically one might use the particle density matrix defined by

$$n^{(1)}(\mathbf{r}, \mathbf{r}') = N_0 \varphi_0^*(\mathbf{r}) \varphi_0(\mathbf{r}') + \sum_{i \neq 0} n_i \varphi_i^*(\mathbf{r}) \varphi_i(\mathbf{r}') \quad (23)$$

, where  $\varphi_i(\mathbf{r})$  are the single particle wave functions and  $n_i$  the occupation numbers. Inserting the plane wave ansatz  $\varphi_{\mathbf{p}_i}(\mathbf{r}) = \frac{1}{\sqrt{V}} e^{i\mathbf{p}_i \cdot \mathbf{r}/\hbar}$  and computing the Fourier transform one can derive the distribution of momentum:

$$n(\mathbf{p}) = N_0 \delta(\mathbf{p}) + \sum_{\mathbf{p}_i \neq 0} n_{\mathbf{p}_i} \delta(\mathbf{p} - \mathbf{p}_i) \quad (24)$$

The distribution exhibits a significant peak at  $\mathbf{p} = 0$  which later was used to observe and prove the Bose Einstein condensation.

## 2 Experimental Realization of BEC

The first actual observation of Bose-Einstein-condensation was achieved by Eric Cornell and Carl Wieman in 1995 at the University of Colorado at Boulder NIST-JILA. They were able to cool Rubidium ( ${}^{87}\text{Rb}$ ) down to  $170\text{ nK}$  and to finally observe the condensation [1]. The low transition temperature results from the very low particle density of this gas with  $n = 2.5 \cdot 10^{12}\text{ cm}^{-3}$  in order to inhibit particle interaction. In this way, a BEC can be induced in a system whose parameters follow the idealized theory and its prediction. In this chapter the way and techniques of producing such low temperatures and the eventual observation will be outlined.

## 2.1 Laser-Cooling

The most convenient and practical way of cooling would be the use of liquid helium, which has a boiling point of 4.2 K. But even with reduction of vapour pressure temperatures with minimum around 1 K can be reached [2], far too high for BEC in matter with the specifications above. Therefore, scientists had to find a new way of cooling matter. In 1975 a cooling mechanism utilizing the monochromatic laser radiation was proposed by Wineland, Dehmelt, Theodor W. Hänsch and Arthur Leonard Schawlow. In principle, this technique makes use of the fact that temperature is related to the average kinetic energy of the atoms in the system. The root mean square velocity can be calculated with  $v_{rms} = \frac{\sqrt{3k_B T}}{m}$ . Laser light decelerates the atoms when scattered because the momentum of photons is transferred. This process can only take place when the atom is moving in the opposite direction of the photon. Assuming the atom has a electric dipole transition at frequency  $\nu_0$ , the laser frequency  $\nu$  is tuned slightly below that value. Moving towards the photon, atoms with certain velocity "see" it at  $\nu_0$  and the probability for scattering is much higher than for atoms moving away from the light source. They are effectively transparent for light. Change of velocity for one scattering event can be easily calculated:

$$\Delta\vec{v} = \frac{\hbar\vec{k}}{M} \quad (25)$$

$\vec{k}$  wavevector of photon  
 $M$  mass of atom

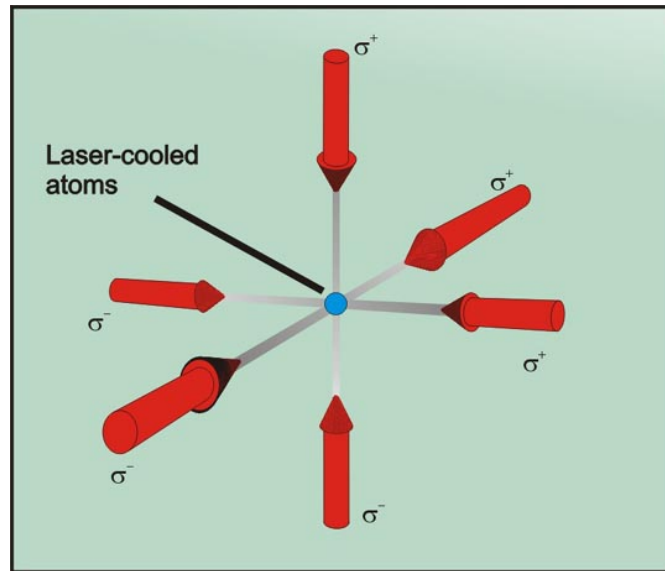


Figure 2: Experimental setup for laser cooling [3]

The absorption frequency can be derived taking into account the Doppler-effect and the energy and momentum conservation, resulting in a recoil term  $R = \frac{(\hbar k)^2}{2M}$ . After

that, the atom is an excited state, where it reemits a photon. Its direction is random, so the occurring recoil cancels out when averaging over many scattering processes. The formulae for absorption and emission yield [4]:

$$\begin{aligned}\omega_{abs} &= \omega_0 + \vec{k}_{abs}\vec{v} - \frac{1}{2}\omega_0\beta^2 + \frac{R}{\hbar}, & \beta &= \frac{|\vec{v}|}{c} \\ \omega_{em} &= \omega_0 + \vec{k}_{em}\vec{v}' - \frac{1}{2}\omega_0\beta^2 - \frac{R}{\hbar}\end{aligned}\quad (26)$$

$\omega_{abs}, \omega_{em}$  frequencies of absorbed and emitted photon  
 $\vec{v}'$  velocity of excited atom

Here, the formula for frequency shift due to Doppler-effect was expanded.

$$\omega' = \omega \frac{\sqrt{1 - \beta^2}}{1 - \beta}$$

Setting the  $\vec{k}_{em}$  zero as explained above, we obtain for the average loss of kinetic energy per atom and per event:

$$\Delta = \omega_{abs} - \omega_{em} = \hbar\vec{k}\vec{v} + 2R \quad (27)$$

$$(28)$$

From (?? we see the detuning of the laser frequency  $\omega_{abs}$  from the resonance frequency  $\omega_0$ , which is necessary for an optimal absorption and hence deceleration of atoms. As we see in the diagram (3), the peak of the spectral intensity distribution of the laser has to be shifted away from the maximum of the Lorentz-shaped absorption spectrum of the atom by  $\omega_{abs} - \omega_0$ , resulting in resonance in the rest frame of the atom only when its moving towards the laser.

Since  $\hbar\vec{k}\vec{v} < 0$ , the modulus of this value has to be larger than  $2R$  for reducing the kinetic energy of the atom according to (27).

Taking, for example, a sample of atoms at 300 K with mass 100 amu and a resonance frequency  $\mu_0 = 5 \cdot 10^{14}$  Hz (which corresponds to  $\lambda = 600$  nm leads to  $v_{rms} = 2.2 \cdot 10^4$  cm/s and eventually to  $\Delta E_{kin} = \frac{3}{2}k_B\Delta T$  with  $\Delta T = 0.012$  K. This implies that more than 10.000 scattering events with a photon are necessary for each atom to decrease the global temperature close to 0 K.

The probability of scattering related to the cross section is given for this process by:

$$\sigma(\omega) = \sigma_0 \frac{(\frac{1}{2}\gamma)^2}{(\omega - \omega_0)^2 + (\frac{1}{2}\gamma)^2} \quad (29)$$

$\sigma_0$  is cross section at resonance frequency  $\omega_0$ . The damping factor  $\gamma$  is related to the finite lifetime in the excited state and so to the quantity for the natural linewidth. With the change in momentum in every scattering event a frictional force is imposed

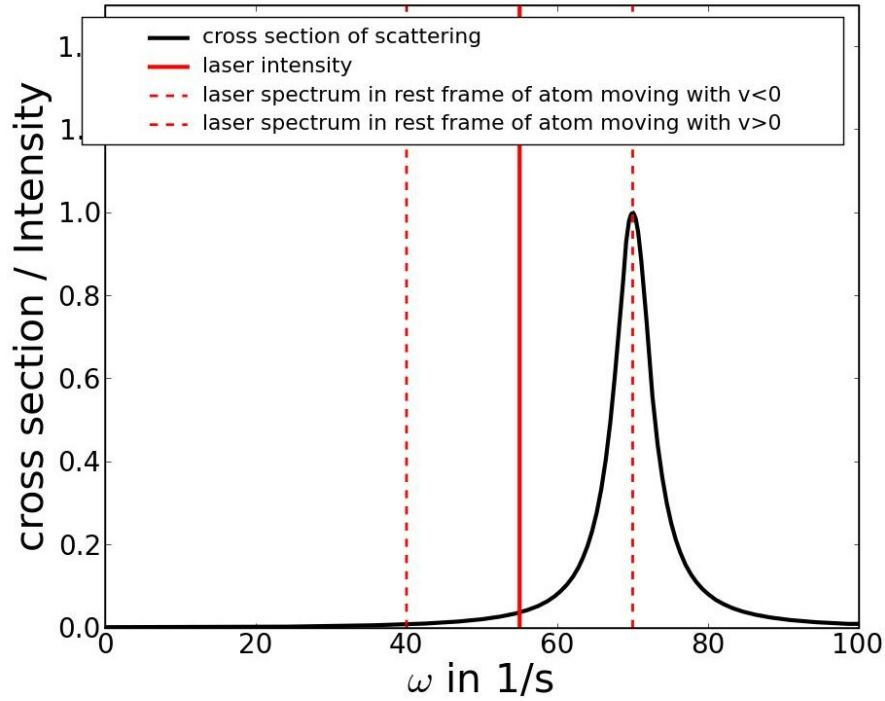


Figure 3: Laser and absorption spectrum of atom, Doppler-shifted lines

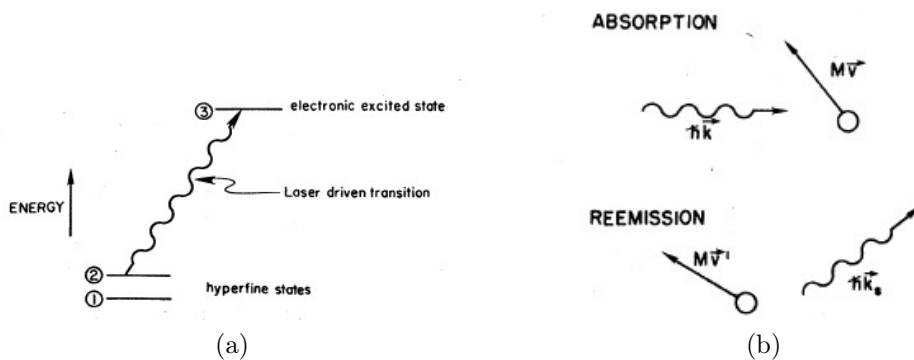


Figure 4: a) Energy-level-diagram for alkali-like-atom, b) Scattering process of laser photon which results in a momentum loss of the scattering atom, [4]

on the atoms:

$$F_x = -\hbar k \times R(I, \Delta)$$

where  $R(I, \Delta)$  is the net absorption rate, depending on the intensity and the detuning.

$$R(I, \Delta) = \frac{\gamma}{2} \left( \frac{I/I_s}{1 + I/I_s + [2(\Delta + kv_x)/\gamma]^2} \right), \quad I_s : \text{saturation intensity} \quad (30)$$

The maximum is reached, when  $\Delta = -kv_x$ , i.e. the Doppler-shift in linear approximation leads to resonance with the atomic transition. Since the atoms moving in opposite direction ( $v_- < 0$ ) have to be decelerated as well, another laser directing inversely is applied. This means a total force  $F_x = F_+ + F_-$ . The index indicates the direction of laser light ( $\pm x$ ). At high temperatures, that means  $k|v_x| \gg \gamma$ , it holds  $F_- \gg F_+$ . At low temperatures, which means  $|kv_x| \ll \Delta$  and  $|kv_x| \ll \gamma$ , the relation takes the simple form [5]:

$$F_x = -\alpha v_x \quad (31)$$

$$\alpha = -\frac{8\hbar k^2 \Delta}{\gamma} \left( \frac{I/I_s}{[1 + I/I_s + (2\Delta/\gamma)^2]^2} \right)$$

With  $\Delta < 0$ ,  $\alpha > 0$  is a damping factor, which leads to a effective cooling rate of:

$$\left( \frac{dE}{dt} \right)_{cool} = F_x v_x = -\alpha v_x^2 \quad (32)$$

Until now we have not taken the heating of the sample into account. An atom with zero mean velocity does not correspond to zero temperature, since the average of the squared velocity is unequal zero. In fact, the particle is performing a Random Walk, where the mean momentum depends on the number  $N$  of interaction events with the 2 laser beams [5].

$$\langle p_x^2 \rangle = 2N(\hbar k)^2 \quad (33)$$

$$N = 2Rt$$

$$\frac{d\langle p_x^2 \rangle}{dt} = 4\hbar^2 k^2 R$$

$$\left( \frac{dE}{dt} \right)_{heat} = \frac{1}{2m} \frac{d\langle p_x^2 \rangle}{dt} = \frac{2\hbar^2 k^2 R}{m}$$

From these equations it is evident that a high intensity of light and an associated high frequency of scattering events result in a larger value for momentum and therefore heating of the medium. An equilibrium between cooling and heating process is reached when  $\left( \frac{dE}{dt} \right)_{heat} = \left( \frac{dE}{dt} \right)_{cool}$ . By means of this condition, one can derive the possible minimum temperature, the so called Doppler limit, assuming again  $|kv_x| \ll |\Delta|$  and

low intensities  $I \ll I_s$ .

$$\begin{aligned}
 -\alpha v_x^2 + \frac{2\hbar^2 k^2 R}{m} &= 0 & (34) \\
 \frac{1}{2}k_B T &= \frac{1}{2}m v_x^2 \\
 \Rightarrow T_{min} &= -\frac{\hbar\gamma}{8k_B} \frac{(1 + I/I_s + 4\Delta^2/\gamma^2)}{\Delta/\gamma} \\
 &\approx \frac{\hbar\gamma}{2k_B}
 \end{aligned}$$

Therefore, typical values of the Doppler limit lie in the  $\mu\text{T}$ -range, since  $\tau = \frac{1}{\gamma}$  usually takes values of several ns. The above derivations was performed only for the 1-D-case (x-direction), which is obvious considering the energy-temperature relation in (34). In fact, lower temperatures are possible considering the spatial variation due to interference of the counter-propagating laser beams. The two Zeeman-sublevels  $M_J = \pm 1/2$  of the ground state  $^2S_{1/2}$  are splitted and the harmonic modulation of their potential energy due to the laser field is  $180^\circ$  phase shifted. A moving atom, which occupies one of these states, follows the modulated potential and converts potential energy in kinetic energy and vice versa. The laser frequency is tuned in that way that the atom can only absorb light when its on top of the hill making a transition into the state  $^2P_{3/2}$ . From there instant transition back into both Zeeman-levels is possible, whereas a change between these levels means an additional energy which the atom has to deduct from its kinetic energy. The minimum temperature according to this process is roughly given by the recoil of the emitting photon, which can be derived from the momentum conservation.

$$\begin{aligned}
 \frac{1}{2}k_B T_{min} &= \frac{p^2}{2m} = \frac{h^2}{2m\lambda^2} \\
 T_{min} &= \frac{h^2}{mk_B\lambda^2} & (35)
 \end{aligned}$$

This technique eventually enables temperatures down to  $2\mu\text{K}$ .

## 2.2 Magnetic trapping

The gas may be cooled down with the previous steps, but still the transition temperature depends on the volume density of atoms according to formula (20). This means that the sample has to be locally confined. The most convenient way in order to prevent interaction with the environment and and the enclosure is magnetic trapping, which makes use of a non-zero magnetic moment of the electric neutral atoms. The simplest structure of those atoms are alkali atoms like Rubidium, where a valence electron occupies the s-orbital ( $l = 0$ ). The other electrons lie in closed shells, so that their total spin and angular momentum cancel out. Since the number of electrons and protons in an alkali atom is odd, the number of neutrons has to be even in order to

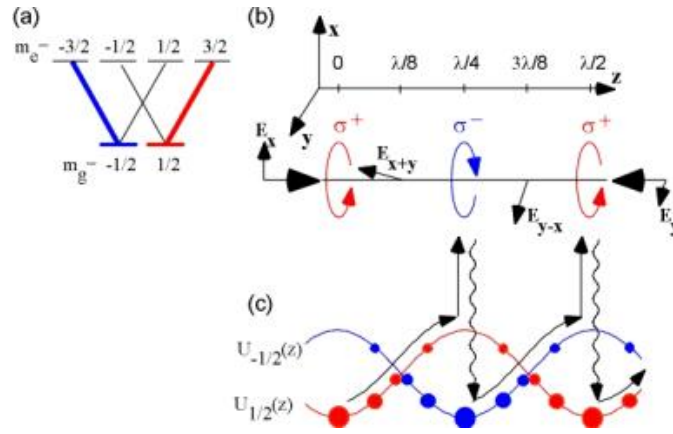


Figure 5: Sisyphus effect [6]

obtain a boson. But this means a non-zero nuclear spin  $I$  which interacts with the valence electron. For the case of Rubidium the spin bzw. angular momenta have the values  $S = \frac{1}{2}$ ,  $L = 0 \rightarrow J = \frac{1}{2}$  and nuclear spin has  $I = \frac{3}{2}$ . They add up to the total angular momentum after the rule of addition of angular momenta:

$$\begin{aligned} \mathbf{F} &= \mathbf{I} + \mathbf{J}, \quad \mathbf{J} = \mathbf{L} + \mathbf{S} \\ F &= I + J, \quad I + J - 1, \dots, |I - J| \\ \rightarrow F &= I \pm 1/2, \quad F = 1 \text{ or } F = 2 \end{aligned} \quad (36)$$

Hyperfine interactions between nuclear spin  $I$  and electron spin  $J$  are satisfied by the term  $H_{hf} = A\mathbf{I} \cdot \mathbf{J}$ . The energy difference between the two hyperfine levels according to (36) yields  $\Delta E_{hf} = A(I + \frac{1}{2})$ . For describing magnetic trapping, the Zeeman-term in the Hamiltonian is crucial.

$$\begin{aligned} \text{magnetic moment : } \quad \boldsymbol{\mu} &= -\mu_B g \mathbf{J} \\ &= \mu_B (g_l \mathbf{L} + g_s \mathbf{S}) \\ \text{perturbation term : } \quad V_M &= -\boldsymbol{\mu} \mathbf{B} \end{aligned}$$

With a magnetic field  $\mathbf{B} = B\mathbf{e}_z$  applied, the perturbation term adopts the following form for alkali atoms:

$$V_M = 2\mu_B J_z B \quad (37)$$

The Hamilton operator therefore becomes:

$$H = A\mathbf{I} \cdot \mathbf{J} + 2\mu_B J_z B \quad (38)$$

The weak interaction of the nuclear moment with the magnetic field was neglected

here. The deviation of the energy for the states  $|F, m_F\rangle$  is given by the matrix element:

$$\begin{aligned} \langle F, m_F | 2\mu_B J_z B | F, m_F \rangle &= g_L \mu_B m_F B \\ g_L &= \frac{(F(F+1) + J(J+1) - I(I+1))}{2F(F+1)} \end{aligned} \quad (39)$$

But these are not the eigenstates of the Hamilton-Operator (38), but the states  $|m_I, m_J = \pm 1/2\rangle$ . Diagonalization of the Hamilton matrix yields eventually the corresponding energy values. For instance, states  $m_F = \pm 2$  are given by  $|\pm 3/2, \pm 1/2\rangle$  and the energies are:

$$\begin{aligned} E_{m=+2} &= \frac{3}{4}A + \mu_B B \\ E_{m_F=-2} &= \frac{3}{4}A - \mu_B B \end{aligned} \quad (40)$$

At high magnetic fields  $C \gg A$ , these levels simply become  $E = \pm \mu_B B$ . This gives a quantity of energy due to the magnetic field, but it does not say for which states these values apply. With respect to (39) one can classify the states into high-field-seeking and low-field-seeking-states. For example, for  $F = 2$  the Lande factor is positive and therefore  $m_F = 1, 2$  is low-field-seeking. The same applies for  $F = 1, m_F = -1$  because the Lande factor is negative in this case. Particularly, in the experiments done by Cornell and Wieman they used a short pulse of circularly polarized laser light to pump all atoms and align their moment to a small magnetic bias. in this way they set  $F = 2, m_F = 2$  [1].

### 2.2.1 Applied magnetic field and evaporative cooling

The apparatus the research group was using (see figure 6) comprised first of all a glass cell with a square base with side length of 2.5 cm and length 12.0 cm, which contained the diluted vapor provided by a chamber at  $T = 300$  K with pressure of  $10^{-11}$  torr. After the laser cooling process described above, a TOP (time orbiting potential)-trap is switched on. Here, two larger coils in anti-Helmholtz configuration create the principal magnetic field  $\mathbf{B}$  which forms the potential bowl for trapping and controlling the gas.

$$\mathbf{B} = B'(x, y, -2z) \quad (41)$$

Only this quantitative formulation of the field implies, that the interaction with magnetic moments of the atoms will not be as straightforward to describe as formula (39) might suggest. To avert this problem, one assumes adiabatic approximation where an atom remains in the same quantum state relative to the momentary direction of the field. As seen in (41), the field vanishes at the centre, so that the low field seeking atoms are gradually driven into the potential minimum. This condition will not hold once they reach the region where the magnetic field vanishes. There, it is possible that the motion of the atom deviates from the direction of the field causing spin-state transitions. A low-field-seeking state suddenly becomes a high field seeking state and

the atom is lost, since it will be repelled by the magnetic trap. To overcome this problem, the experimental set up was added with 4 smaller coils perpendicular to the Helmholtz coils. Each one placed in one of the four remaining directions, so that the coil configuration looked like a cuboid. They imposed a small transverse rotating field of amplitude  $B_0$  and frequency  $\omega = 2\pi \cdot 7.5 \text{ kHz}$ . By averaging the resulting field  $\mathbf{B}$  over time and calculating and expanding the modulus, one can derive the form of potential  $V$  created by the magnetic field. The value in the centre is now nonzero which ensures the preservation of atoms.

$$\mathbf{B} = (B'x + B_0 \cos \omega t, B'y + B_0 \sin \omega t, -2B'z) \quad (42)$$

$$\bar{B} = B_0 + \frac{B'^2}{4B_0}(x^2 + y^2 + 8z^2)$$

$$V = g_L \mu_B m_F B$$

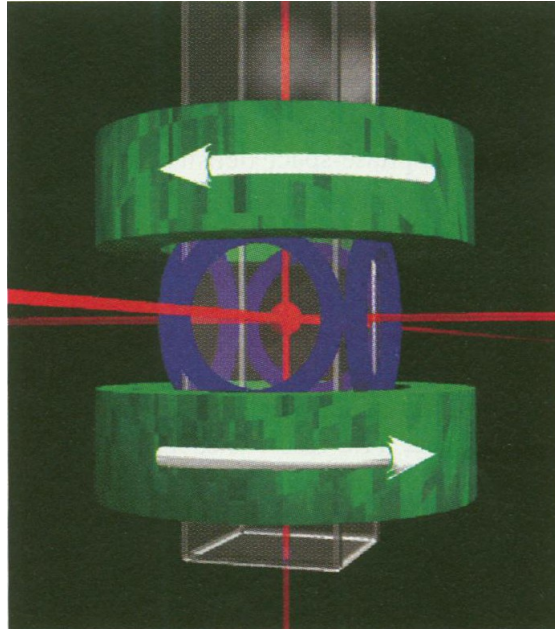


Figure 6: Principal setup of the Cornell-Wieman-experiment [1]

This is a harmonic potential providing confinement for the condensate. Until this point the experiment point is conducted in that way, that atoms from a Rubidium source are collected in the MOT and cooled with laser cooling down to  $20 \mu\text{K}$  within 300 s. After that the atoms are pumped into the low-field seeking state  $F = 2$ ,  $m_F = 2$  and the laser light is removed. Afterwards, the quadrupol and the transverse rotating field is applied, whereas the quadrupol field has to be ramped slowly to its maximum in order to prevent spin state transition. The temperature increased here to 90 K. Up to this point, a density up to  $2^{10} \text{ cm}^{-3}$  was achieved, but far too high for the transition temperature of  $\sim 170 \text{ nK}$  [5]. The last step, the evaporative cooling, comprises another magnetic field irradiated as radio waves. Monochromatic waves  $\omega_{r,f}$  are tuned in that way that they induce a spin-flip of atoms with high energy. These

atoms sample regions of high magnetic field which shifts the distance of Zeeman-levels and consequently makes possible to select them spectroscopically from the the low energy atoms. Once removed from the high energy part, the cloud rethermalizes at a lower temperature and phase-space density increases. The radio frequency was ramped down continually, starting from about  $2\pi \cdot 10$  MHz [7] and ending at  $\nu_{evap}$ . This last frequency relates to the maximum energy an atom can have and is therefore linked with the final temperature. Consequently, if  $\nu_{evap}$  is chosen small enough, Bose-Einstein-condensation can take place.

### 2.3 Observation of BEC

For the observation, the field forming the trap was almost switched off and the cloud was let to expand for 60 ms. After the cloud was exposed to a circularly polarized laser pulse for 20  $\mu$ s, which is resonant with the  $5S_{1/2}(F = 2) \rightarrow 5P_{3/2}(F = 3)$  transition, the absorption image was finally recorded. The intensity on the image is related to the density of atoms at this point. Thus, the picture provides the coordinate-space distribution which is equivalent to velocity distribution. Repeating the cooling procedure and decreasing with each cycle  $\nu_{evap}$ , the group observed the appearance of a peak in the velocity distribution in the centre at  $\nu_{evap} = 4.23$  MHz which is related to the macroscopic occupation of the ground state. Further decrease of  $\nu_{evap}$  diminishes the noncondensate fraction and makes the peak appear clearer and sharper (see the picture). The sample parameters for observation such as  $T = 170$  nK are taken shortly before condensation at  $\nu_{evap} = 4.25$  MHz. The number density gave  $2.6 \cdot 10^{12} \text{ cm}^{-3}$ .

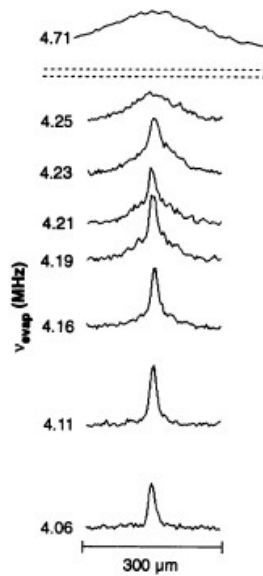


Figure 7: velocity distribution for different values  $\nu_{evap}$ , [1]

Considering the projection of the velocity distribution onto the image, the central peak does not adopt an ideal circular shape, but elliptical shape. This fact results

from an anisotropy in the confining potential. The dimension of the anisotropy is additionally modified by the interaction of particles which were not taken into account at any point in the derivations of the corresponding formulae.

### 3 Subsequent experiments

#### 3.1 Observation of BEC in a gas of sodium atoms

In an experiment at the MIT, Cambridge, in September 1995 the condensation of sodium atoms was observed. Scientists were able to utilize a new trap to obtain much higher phase-space densities. The problem of zero field in the center of a spherical quadrupol field, where atoms get lost, is here solved with a laser beam focused at the centre. This laser is blue detuned to reduce heating due to scattering. Atoms are now repelled from this region, called optical plug, because of the optical dipol force. In the same way like the first experiment, the high energy atoms were removed using rf-radiation which induces spin flip at the rim of the potential. Since the atoms are transformed into untrapped states, which are attracted by high field, the potential bends over in the view of these atoms. The whole potential is presented in figure (8)

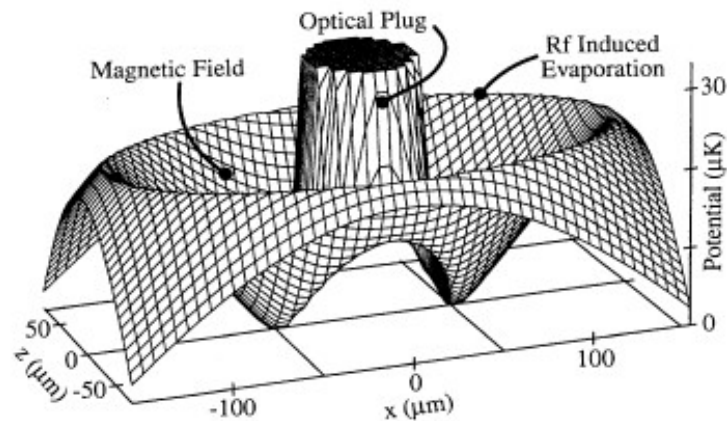


Figure 8: confining potential for observation of BEC in sodium [8]

For imaging, a time-of-flight picture of the cloud was taken. First, a laser pumped the atoms from the  $F = 1$  to the  $F = 2$ -state. Later they changed to the  $F = 3$ -state with a  $100 \mu\text{s}$ -laser pulse in  $y$ -direction. Its image was recorded onto charged-couple device with a resolution of  $8 \mu\text{m}$ . Similarly to the experiment with Rubidium, under a certain rf frequency  $\nu_{rf}$  an elliptical core appeared. It consists of the ground state atoms and lies within the spherical cloud of uncondensed atoms. The critical frequency was  $0.7 \text{ MHz}$  and based on time-of-flight-images a temperature of  $2.0 \pm 0.5 \mu\text{K}$  could be estimated. Integration over the absorption image delivered the parameters of the condensate at the transition point. The number reached  $5 \cdot 10^5$  and the number density  $4 \cdot 10^{14} \text{ cm}^{-3}$  [8].

### 3.2 Observation of interference between two Bose condensates

Until now, absorption technique was used to image the Bose condensates. The probe light was almost completely absorbed and added to heating of the sample through recoil energy. A new way of imaging is phase contrast imaging, well-known from microscopy. In contrast to absorption, the probe light is detuned from resonant transition, e.g. 1.77 GHz. The photons are scattered in forward direction, being retarded in phase compared to the unscattered light. In other words, the spatial distribution of the refractive index divides the probe light into a surround (S) and defractive (D) fraction. Through a  $\frac{\lambda}{4}$ -phase plate in the objective rear focal plane, the S-wave is advanced by  $\frac{\pi}{2}$  phase angle or the D-wave is retarded by that amount. The image is formed by the interference of these two waves providing good signal-to-noise ratio, since the probe light with its negligible contribution to heating can be employed in a much higher magnitude. Phase contrast imaging was used to take "real-time-movies" of collective excitations of Bose gas. These were applied by periodically moving the center of the trap, resulting in a dipole mode of the condensate, where the entire cloud is oscillating along an axis in the trap. The frames of such a movie are separated by 10 msec. Phase contrast imaging was brought into play when observing the formation of two Bose condensates in a double well potential. The experimental setup was nearly the same as for the BEC-experiment with sodium. The potential was made up by a similarly overleaf magnetic trap, where the argon ion laser was focused in the center of the trap, separating the two condensates. Their distance could be controlled by changing the argon ion laser power between 7 and 43 mW. The observation was conducted in the same way as described above. The trap and the argon laser were switched off and the expanding cloud was pumped and probed by excitation into the  $F' = 3$  state. The probe beam was collinearly with the argon laser beam here.

The interference pattern can be seen in picture (9), which clearly comprises of fringes. The two condensates were treated as point-like pulsed sources, where the fringe period can be computed as follows [9]:

$$\lambda = \frac{ht}{md} \quad (43)$$

$d$  distance of the two sources

$m$  mass of atoms

$t$  time between switching of potential and observation

The time-of-flight was chosen in all pictures as 40 ms resulting in fringe spacings of  $\sim 15 \mu\text{m}$ . The experimental values of fringe spacing are in good consistency with the theoretical prediction. To prove that the interference pattern is caused by the interaction of two Bose condensates, only one part was illuminated and observed. Hereby, the corresponding absorption image matched one side of the picture of a double condensate, but does not cover or explain structures of the interference part in the middle (figure 11). In conclusion, the experiment proved the matter-wave properties of the ground-state and the spatial coherence leading to interference over an area as

large as the condensate.

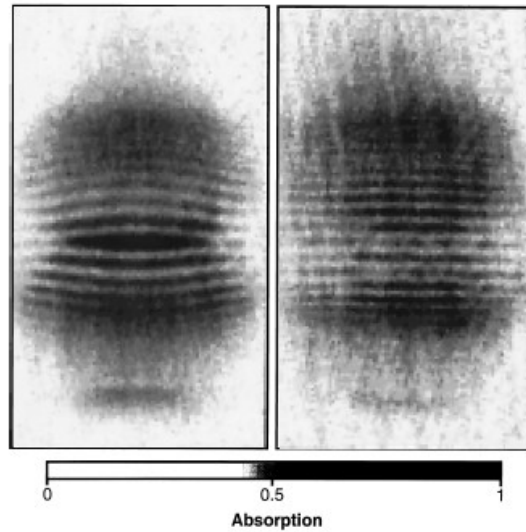


Figure 9: interference pattern of two Bose condensates for 3 and 5 mW power of argon ion laser [9]

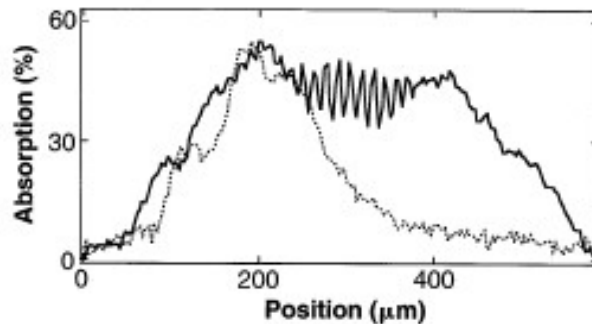


Figure 10: time of flight image of a single (dotted) and double condensate (solid) [9]

### 3.3 Superradiant Rayleigh Scattering from a Bose-Einstein Condensate

Interesting phenomena occur when coherent laser light interacts with the coherent ground state of a Bose condensate. The following experimental and theoretical propositions are related to a paper of the Prichard and Ketterle group [10]. Basically, a photon with momentum  $\mathbf{k}_0$  is scattered by an atom in the ground state into the momentum state  $\mathbf{k}_i$  imparting a recoil momentum  $\hbar\mathbf{K}_j = \hbar(\mathbf{k}_0 - \mathbf{k}_i)$ . This wave interferes with the condensate and forms a grating, where following photons are diffracted, producing further  $\mathbf{K}_j$ -matter waves. The condensate is modulated with the amplitude

$N_{mod} = 2\sqrt{N_j N_0}$ , where  $N_j$  is the number of recoiled atoms and  $N_0$  the number in the condensate. Since we have a connection between the total power of scattering photons in the phase matching direction  $\mathbf{k}_i$  with the number  $N_{mod}$ ,

$$P = \hbar\omega f_j R \frac{N_{mod}^2}{4} \quad (44)$$

we can derive quantum-mechanically the rate of scattered photons  $P/\hbar\omega$  and therefore the change over time for  $N_j$

$$\dot{N}_j = RN_0 \frac{\sin^2 \theta_j}{8\pi/3} \Omega_j (N_j + 1) \quad (45)$$

$$\Omega_j = \int d\Omega(\mathbf{k}) \left| \int \tilde{\rho}(\mathbf{r}) e^{i(\mathbf{k}_i - \mathbf{k}) \cdot \mathbf{r}} d\mathbf{r} \right|^2$$

with :  $|\mathbf{k}| = |\mathbf{k}_i|$ ,  $\tilde{\rho}(\mathbf{r})$  spatial density distribution

The integral  $\Omega_j$  is a maximum when the light is emitted in the direction of the largest extend of the condensate, the so called "end-fire mode". The experimental setup comprised a magnetic trap of several million sodium atoms ( $3S_{1/2}$ ,  $F = 1$ ) condensed into a cloud of  $20 \mu\text{m}$  diameter and  $200 \mu\text{m}$  length. The laser-light was red-detuned from resonance with the transition to the states  $3P_{3/2}$ ,  $F = 0, 1, 2$ . The laser power was set to reach Rayleigh scattering rates of  $4.5 \cdot 10^1 - 4.5 \cdot 10^3 \text{ s}^{-1}$ . After a pulse of up to  $800 \mu\text{s}$  duration and several ms time of flight, the scattered atoms were probed. The result depended on the angle  $\theta_j$  between polarisation of incident light and direction of emission.

To examine the behaviour of the system under a square shaped laser pulse, a photomultiplier was placed around the axial direction of the condensate to determine the rate of scattered photons in this direction. The rise of intensity, which should follow equation (46), was constant with increasing laser intensity for small intensity until it passed a threshold and the inversed rise time began to increase; superradiance occurs. The explanation for this is, that for  $N_j \ll 1$  equation (46) becomes  $\sum_j \dot{N}_j = RN_0$ , normal Rayleigh scattering at a constant rate. Once the  $N_j$  fraction becomes substantial, we are in the superradiant regime. We can therefore rewrite the equation by adding a loss term  $L_j$  to the gain  $G_j$ , taking into account the observation of a threshold.

$$\dot{N}_j = (G_j - L_j)N_j \quad (46)$$

The normal Rayleigh scattering rate  $R$  was measured by using parallel polarization ( $\theta_j = 0$ ) to suppress the dominant anisotropic scattering in direction of the long axis and integrating the emitted intensity over the whole space. The loss rate  $L_j$  could be determined from the offset in the inverse rise time diagram, which yielded  $1/L_j = 35 \mu\text{s}$ . It can be interpreted as the decoherence time for matter wave interference. In conclusion, this experiment demonstrated that spontaneous emission in a Rayleigh scattering process of a laser beam at a Bose condensate creates a matter-wave grating through the recoiling atoms, where subsequent photons are coherently

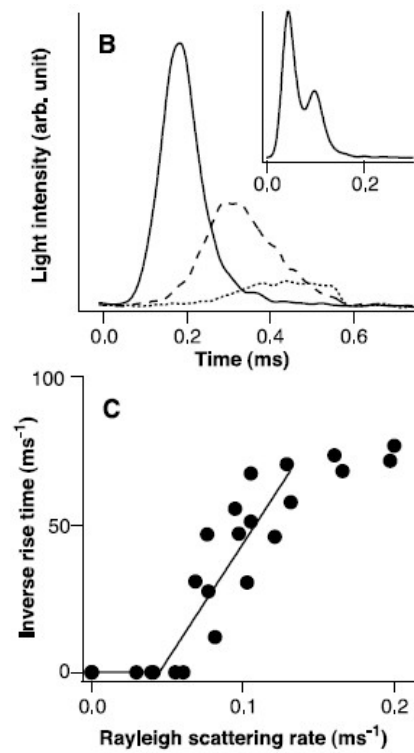


Figure 11: time-resolved evolution of scattered photon intensity and observation of threshold for occurrence of superradiance (faster rise in intensity of scattered light) [10]

scattered. The matter wave grating induces therefore a stimulated emission of photons in certain direction and a production of atoms with a certain recoil, forming a superradiant cloud.

As described above, the condensates has long-range coherence, but whether the same applies for the superradiant cloud was yet to be shown. Another experiment at the National Institute of Standards and Technology in Gaithersburg, MD (NIST) examined this question. The experimental setup comprised  $2 \cdot 10^5$   $^{87}\text{Rb}$  atoms in a dc-magnetic trap, where the condensate adopts a highly elongated shape [11]. Along this axial direction the laser was applied, detuned with  $-2\text{GHz}$  from the  $5S_{1/2}, F = 1 \rightarrow 5P_{3/2}F' = 2$  transition. Likewise, the dominant emission mode is the end-fire mode causing the photons to backscatter and to impart a momentum of  $2\hbar k$ . This superradiance process as well as the one in the previous experiment has its origin in a spontaneous emission and therefore a random phase. Thus, it can not be used in amplifying already existing matter-waves, consequently in realising an atom laser, the major aim of the scientists. For this, a seed-matter needed to be created, which will be amplified later by the superradiant effect. This seed with a sharp momentum could be obtained through Bragg diffraction demonstrated by the same research group in an earlier paper [12]. Here, two counter-propagating laser beams, which are detuned from the transition stated above, intersect at the position of the condensate (here Sodium was used instead of Rubidium). The wavelength of the two laser deviate slightly from each other, so that they form a moving standing wave, where the condensate can be scattered.  $n$ th order Bragg diffraction in this case can be seen as stimulated  $2n$ -Raman process, where a photon of one beam is absorbed and then stimulated emitted into the other beam, while in this process a momentum  $P_{recoil}$  is imparted, adding up to a final momentum  $n \cdot P_{recoil}$  of the atom. Conservation of energy gives a condition for the detuning  $\delta_n$  of the two lasers.

$$\frac{(nP_{recoil})^2}{2M} = n\hbar\delta_n \quad (47)$$

$$P_{recoil} = 2\hbar k \sin \theta/2 \quad \text{recoil momentum}$$

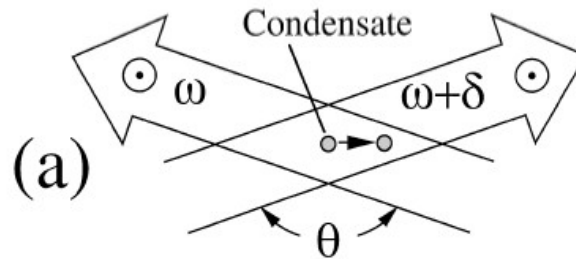


Figure 12: laser beams and condensate in a setup to coherently split the condensate [12]

In case of the setup for producing the Rubidium matter-wave seed, the lasers (Bragg

beams) were counter-propagating ( $\theta = 180^\circ$ ) making a frequency shift of  $\Delta\omega = 15$  kHz necessary for first-order ( $n = 1$ ) Bragg diffraction. Under irradiation of the two lasers the momentum space wavefunction will oscillate between the two levels  $|g\rangle = |p = 0\rangle$  and  $|e\rangle = |p = 2\hbar k\rangle$ , where under adjusting intensity and pulse duration a arbitrary amount can be transferred into the excited momentum state. In this basically two level system a  $\pi/2$  ( $\pi$ ) pulse excites half (all) atoms of the condensate. In detail:

$\pi/2$ -pulse

$$\begin{aligned} |g\rangle &\rightarrow \frac{1}{\sqrt{2}}(|g\rangle - e^{-i\varphi}|e\rangle) \\ |e\rangle &\rightarrow \frac{1}{\sqrt{2}}(e^{i\varphi}|g\rangle + |e\rangle) \end{aligned}$$

$\pi$ -pulse

$$\begin{aligned} |g\rangle &\rightarrow e^{-i\varphi}|e\rangle \\ |e\rangle &\rightarrow e^{i\varphi}|g\rangle \end{aligned}$$

with  $\varphi$  being the phase of the moving standing wave in the centre of the condensate and in the middle of the pulse [13]. For example, a pulse duration of  $15 \mu s$  transferred 6.5 % of the atoms into the  $|2\hbar k\rangle$  state. The experiment proceeds by extinguishing the magnetic trap and applying the Bragg pulses for this time period. Afterwards, the superradiance pulse A amplifies the seed wave whereas the population of this  $|2\hbar k\rangle$  state is controlled by the duration of the pulse.

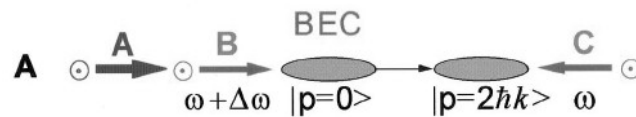


Figure 13: arrangement of condensate and superradiance (pulse A) and Bragg (pulses B, C) laser beams [11]

To prove that the phase of the superradiant cloud is locked to the one of the seed matter wave, the experimenters realized something like a Mach Zehnder Interferometer by setting the population of the moving and resting cloud each 50 % (state:  $\frac{1}{\sqrt{2}}(|g\rangle - |e\rangle)$ ), then applying a second Bragg  $\pi$ -pulse after the clouds were well separated. A  $\pi$ -pulse acts like a mirror and switches the momenta of the clouds which therefore converge (state:  $-\frac{1}{\sqrt{2}}(|g\rangle + |e\rangle)$ ). In the moment of complete overlapping a final  $\pi/2$ -Bragg pulse like the first one illuminated the matter except that the phase of the moving standing wave is altered by  $\phi$ .

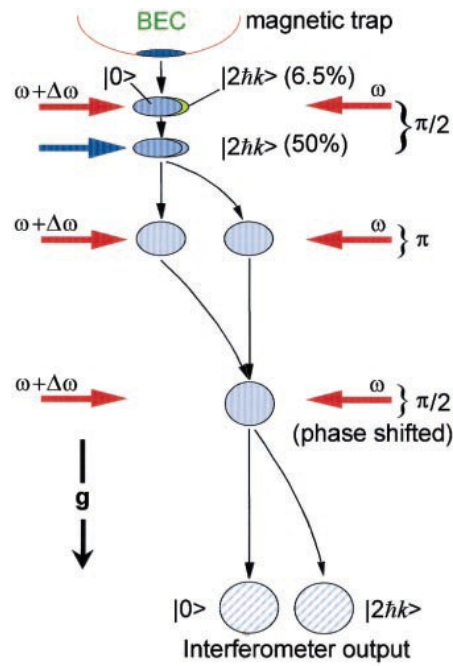


Figure 14: Realisation of a Mach-Zehnder-Interferometer with two condensate clouds by a sequence of Bragg pulses (red) and a superradiant pulse (blue)  
 the clouds are moving after release from the trap due to gravitation [11]

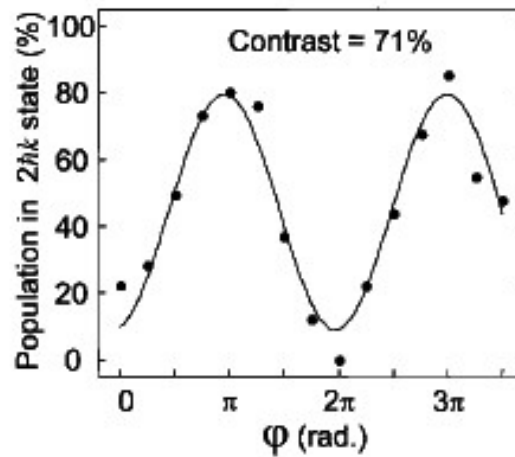


Figure 15: Interferogram showing population of  $|2\hbar k\rangle$  state in dependence of phase deviation  $\varphi$  [11]

If no phase change is applied, all atoms will be in the original  $|g\rangle$  state. If  $\phi \neq 0$  the final state gives  $-\frac{1}{\sqrt{2}}((1 + e^{i\phi})|g\rangle + (1 - e^{-i\phi})|e\rangle)$ . Thus, the probability of finding atoms in the  $|e\rangle = |2\hbar k\rangle$  state would be  $1/2 \cdot (1 - \cos \phi)$ . An experiment, where the population is measured in dependence from  $\phi$ , provides indeed interferometer fringes depicted in (15). Therefore, the superradiant wave phase is locked to the seed wave. Consequently, all properties of a laser regarding amplification, spectral line width, and at least long range coherence has been shown giving rise to the development of the a first atom laser and to the examination of its features.

## Conclusion/Summary

The here stated steps in development of the atom laser consider only roughly the fundamentals and not the technical implementation and application of an atom laser such as interferometry and holography. Here, waves have a much smaller de-Broglie-wavelength which improves the image resolution. Nonetheless, the starting point for the endeavour of creating a Bose-Condensate was still the confirmation of a seventy year old prediction which was published early in the development of quantum theory. This assumption was derived from the Maxwell-Boltzmann distribution, and along with Fermi-Dirac-distribution it formed the base of many models especially in solid state physics. A proof of its validity and consistency was crucial, but realisation seemed to be a major obstacle due to the necessary ultra low-temperatures. A first step in approaching this goal was the invention of a Laser and the subsequent technique of laser-cooling. Since this was not sufficient enough, the technique of magnetic trapping was refined and many suggestion how to magnetically trap atoms had been published. After the solving the problem of too great losses in the trap, the last step of evaporatively cooling the matter followed immediately. The observation of BEC, however, apparently facilitated the efforts on BEC in the first place which can be seen from the slope in the number of papers published on that topic. Next was the successful observation in Sodium, Lithium, Hydrogen and so on, beside Rubidium in the first experiment. Shortly after that, scientists also examined the coherent properties of the ground state with the observation of interference between two Bose condensates. The coherent amplification of a seed wave matter through a Bose condensate, by means of an analogous technique to stimulated emission in optics, was realized shortly afterwards. It could be shown that the amplified cloud exhibits coherence as well, making a condensate in the ground state a promising reservoir for further research on the realisation of a practicable the atom laser.

## Acknowledgement

I want to thank Dr Binoy Sobnack for helping and supervising this literature project. Alone it would have been much more difficult to narrow down the topic on a basic outline as it is presented here, since Bose Einstein condensation has been developed into a broad and scientific interesting area.

---

## References

- [1] Anderson, M. H., J. R. Ensher, M. R. Matthews, C. E. Wieman, and E. A. Cornell: *Observation of bose-einstein condensation in a dilute atomic vapor*. Science, 269(5221):198–201, 1995.
- [2] Clintock, Mc, Meredith, and Wigmore: *Matter at low temperatures*. Blackie & Son Limited, 1984.
- [3] *Working group 4.43: Optical clocks with trapped ions*. [www.ptb.de/en/org/4/44/443/kuehl\\_e.htm](http://www.ptb.de/en/org/4/44/443/kuehl_e.htm).
- [4] Wineland, D. J. and Wayne M. Itano: *Laser cooling of atoms*. Phys. Rev. A, 20(4):1521–1540, Oct 1979.
- [5] Fox, Mark: *Quantum optics: an introduction*. Oxford University Press, 2006.
- [6] *Sub-dopplerkühlung*. <http://www.pi5.uni-stuttgart.de/lehre/hauptseminar2001/Laserkuehlung/html/sub.htm>.
- [7] Petrich, Wolfgang, Michael H. Anderson, Jason R. Ensher, and Eric A. Cornell: *Stable, tightly confining magnetic trap for evaporative cooling of neutral atoms*. Phys. Rev. Lett., 74(17):3352–3355, Apr 1995.
- [8] Davis, K. B., M. O. Mewes, M. R. Andrews, N. J. van Druten, D. S. Durfee, D. M. Kurn, and W. Ketterle: *Bose-einstein condensation in a gas of sodium atoms*. Phys. Rev. Lett., 75(22):3969–3973, Nov 1995.
- [9] Andrews, M. R., C. G. Townsend, H. j. Miesner, D. S. Durfee, D. M. Kurn, and W. Ketterle: *Observation of interference between two bose condensates*. Science, 275:637, 1997.
- [10] Inouye, S., A. P. Chikkatur, D. M. Stamper-Kurn, J. Stenger, D. E. Pritchard, and W. Ketterle: *Superradiant Rayleigh Scattering from a Bose-Einstein Condensate*. Science, 285(5427):571–574, 1999.
- [11] Kozuma, Mikio, Yoichi Suzuki, Yoshio Torii, Toshiaki Sugiura, Takahiro Kuga, E. W. Hagley, and L. Deng: *Phase-Coherent Amplification of Matter Waves*. Science, 286(5448):2309–2312, 1999.
- [12] Kozuma, M., L. Deng, E. W. Hagley, J. Wen, R. Lutwak, K. Helmerson, S. L. Rolston, and W. D. Phillips: *Coherent splitting of bose-einstein condensed atoms with optically induced bragg diffraction*. Phys. Rev. Lett., 82(5):871–875, Feb 1999.
- [13] Torii, Y., Y. Suzuki, M. Kozuma, T. Kuga, L. Deng, and E.W. Hagley: *Mach-zehnder bragg interferometer for a bose-einstein condensate*. arXiv:cond-mat/9908160v2, 1999.